Coupling Quantum Tunneling with Cavity Photons

Peter Cristofolini,[1] Gabriel Christmann,[1] Simeon I. Tsintzos,[1,2] George Deligeorgis,[2] George Konstantinidis,[2] Zacharias Hatzopoulos,[2] Pavlos G. Savvidis,[2,3] Jeremy J. Baumberg[1]*

[1]NanoPhotonics Centre, Cavendish Laboratory, University of Cambridge, Cambridge CB3 0HE, UK. [2]FORTH-IESL, P.O. Box 1527, 71110 Heraklion, Crete, Greece. [3]Department of Materials Science and Technology, University of Crete, P.O. Box 2208, 71003 Heraklion, Greece.

*To whom correspondence should be addressed. E-mail: jjb12@cam.ac.uk

Tunneling of electrons through a potential barrier is fundamental to chemical reactions, electronic transport in semiconductors and superconductors, magnetism, and devices such as THz-oscillators. While typically controlled by electric fields, a completely different approach is to bind electrons into bosonic quasiparticles with a photonic component. Quasiparticles made of such light-matter microcavity polaritons have recently been demonstrated to Bose-condense into superfluids, whereas spatially-separated Coulomb-bound electrons and holes possess strong dipole interactions. Using tunneling polaritons we connect these two realms, producing bosonic quasiparticles with static dipole moments. Our resulting three-state system yields dark polaritons analogous to those in atomic systems or optical waveguides offering new possibilities for electromagnetically-induced transparency, room temperature condensation and adiabatic photonic to electronic transfer.

Strong coupling of photons to the interband exciton transition in a semiconductor microcavity leads to the formation of polaritons, bosonic quasiparticles whose properties are governed by their mixed light-matter composition. Owing to their quantum indistinguishability and the interplay of their Coulomb interactions, microcavity polaritons show unusually strong light-matter interactions and many-body quantum effects. In particular their small effective mass allows observation of quantum degeneracy effects at temperatures from 10-300K, such as Bose-condensation (*1–4*) and superfluidity flow dynamics (*5*), while their tuneable interactions make them ideal candidates for future quantum optoelectronic devices (*6*) working at room temperature (*7*). By contrast, spatially separating the electron and holes in coupled double quantum wells yields indirect excitons with long-enough lifetime for thermalisation and a large static dipole moment (*8*) allowing for efficient in-plane electrostatic traps (*9, 10*) and the coherent control of electron spins (*11*). By embedding double quantum wells inside a conventional microcavity in the strong coupling regime, we unite the concepts of indirect excitons and microcavity polaritons to produce optically-active quasiparticles with transport properties, named *dipolaritons*. These offer the advantages of both systems: electrical trapping and tuning of excitons, strong optical coupling to low-mass quasiparticles with large de Broglie wavelength, and excellent control over the dipole properties and interactions (*12, 13*).

Microcavities are formed from *p-i-n* semiconductor multilayers surrounded by doped multilayer (DBR) mirrors (*7*) (Fig. 1A; details in supplementary materials) and pumped with a non-resonant laser. Quantum wells (QWs) of InGaAs inside the cavity are arranged in asymmetric pairs separated by a thin barrier (of width L_B) that allows electrons to tunnel between the two wells (Fig. 1A). The wide energy separation of hole states between wells and their large mass means inter-well hole tunneling plays no role and only the low-energy left QW (LQW) hole state is considered. Without tunneling there are two types of exciton in this system. The direct exciton $|DX\rangle$ has both electron and hole in the

left QW (Fig. 1B, top) and so strongly couples to the cavity mode, with its induced dipole moment oriented randomly in the QW plane. The indirect exciton $|IX\rangle$ has the hole in the left QW and the electron in the right QW, thus possessing an additional static dipole moment aligned perpendicularly to the plane, and has very small overlap of electron and hole wavefunctions hence small oscillator strength. When a bias voltage is applied to bring the electron levels in resonance, the electron states in the two QWs mix to give symmetric and antisymmetric electron wavefunctions (red in Fig. 1A), which together with the low-energy hole states (blue) in the left QW produce the exciton modes $(1/\sqrt{2})(|IX\rangle \pm |DX\rangle)$, split by the tunneling energy $\hbar J$. These modes combine the large oscillator strength of the DX with the large static dipole moment of the IX (Fig. 1B, lower).

Embedding DX and IX excitons in the microcavity with cavity mode C now forms a three-state system similar to the atomic Λ-scheme (*14, 15*) which is coupled optically by the vacuum Rabi frequency Ω, and electronically by the electron tunneling rate J (Fig. 1C). While J, Ω are intrinsic to the microcavity design, full control of the dipolariton modes is possible through bias voltage control of tunneling and angle tuning of the cavity mode. In the strong coupling regime, when J is larger than the carrier escape rate from the coupled QW and Ω is faster than the photon decay rate, the system displays three distinct eigenmodes: the lower (LP), middle (MP) and upper (UP) dipolaritons. Thus a conventional microcavity polariton (Fig. 1D, black) can be simply bias tuned to yield the dipolariton spectrum (red) in the strong tunneling regime.

The bias dependence of the photoluminescence (PL) of a $L_B = 4$ nm barrier mesa (Fig. 2) clearly reveals these three dipolariton modes. Because in-plane wavevectors k are conserved, photons emitted at an angle θ directly measure dipolaritons at k. At normal incidence (Fig. 2, A and C) the narrow cavity mode is detuned below the excitons while at 35° (Fig. 2, B and D) the uncoupled modes are all degenerate. For higher electric fields the PL emission weakens because electrons escape the coupled QW system before they can recombine radiatively with a left QW hole, and eventually two of the modes vanish leaving only the most cavity-like dipolariton. A simple harmonic oscillator model coupling the modes $\{|IX\rangle, |DX\rangle, |C\rangle\}$ gives a deeper understanding of these dipolaritons. The Hamiltonian H is

$$H = \hbar \begin{pmatrix} \omega_{IX} & -J/2 & 0 \\ -J/2 & \omega_{DX} & -\Omega/2 \\ 0 & -\Omega/2 & \omega C \end{pmatrix} \quad (1)$$

where $|DX\rangle$ couples to both $|IX\rangle$ and $|C\rangle$, while there is no direct interaction between $|IX\rangle$ and $|C\rangle$ (Fig. 1C) (*16*). Independent control over all parameters in this model is practical: angle-tuning shifts the cavity frequency, bias voltage tunes both the IX (directly) and DX levels (due to the quantum confined Stark effect), the barrier width sets the intrinsic tunneling rate J, and Ω is set by the microcavity design and
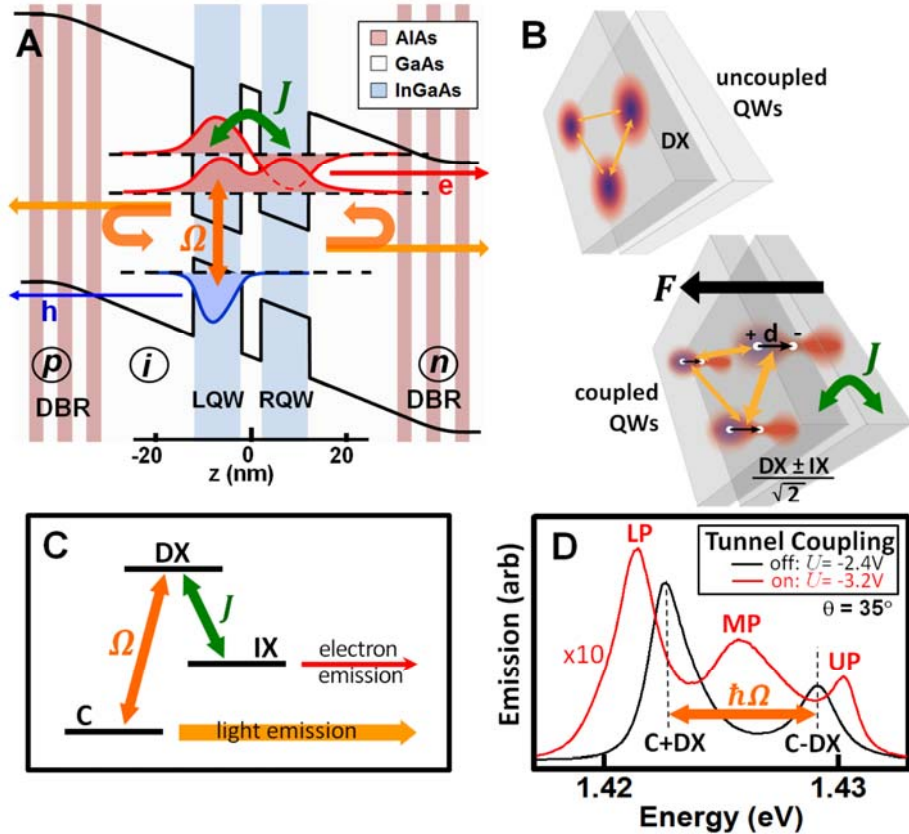
Fig. 1. (**A**) Schematic band structure of coupled quantum wells in a microcavity at tunneling resonance. Due to tunneling coupling *J*, electrons (red wavefunctions) extend over both wells while holes (blue) are confined in the LQW. Strong optical coupling to cavity photons Ω, gives rise to dipolaritons. (**B**) Conventional in-plane excitons (top) acquire a static out-of-plane dipole moment at resonance (bottom). (**C**) Three-level Λ-scheme coupling cavity C, direct DX and indirect IX exciton modes by classical intense laser pump Ω and quantum tunneling *J*. (**D**) Spectra of standard polaritons (black) and dipolaritons (red) tuned with bias.
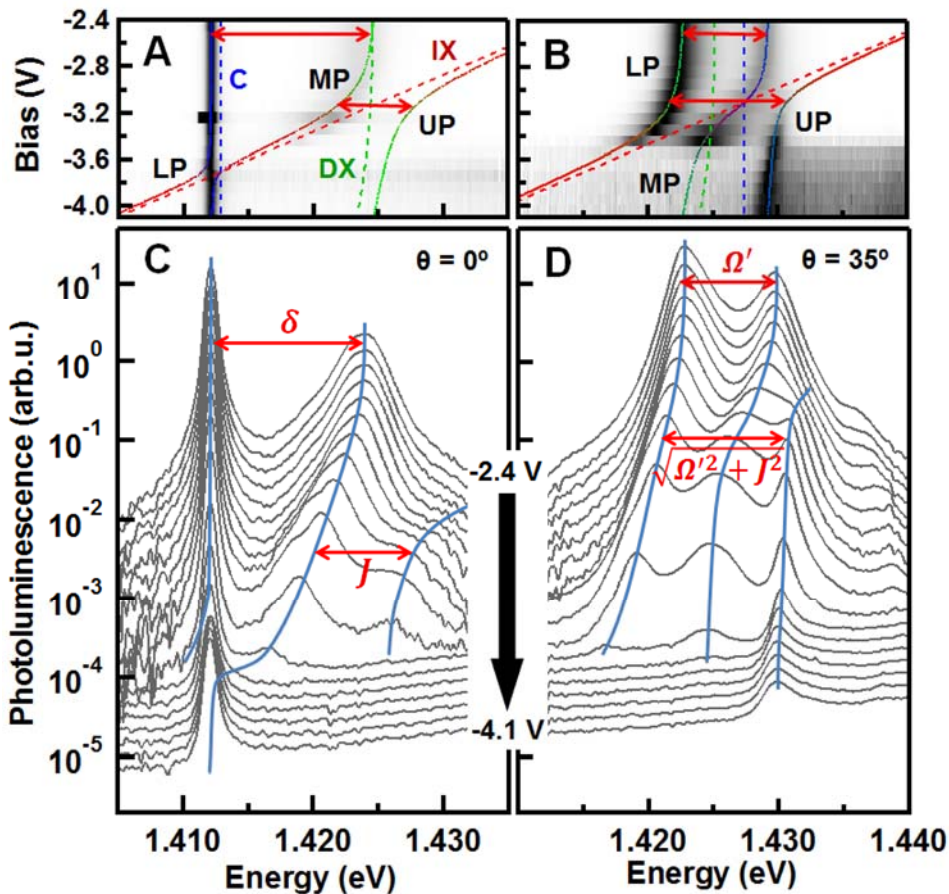
Fig. 2. Normalised PL spectra with bias voltage for (**A** and **C**) the off-resonant cavity and (**B** and **D**) close to resonance for a mesa with L_B = 4 nm. Polariton lines LP, MP and UP in (**A**) and (**B**) are fits to the coupled oscillator model Eq. 1, dashed lines show the uncoupled modes: cavity (C, blue), direct (DX, green) and indirect (IX, red) excitons. In (C) and (D) the spectra are shifted for clarity, blue lines are guides to the eye.
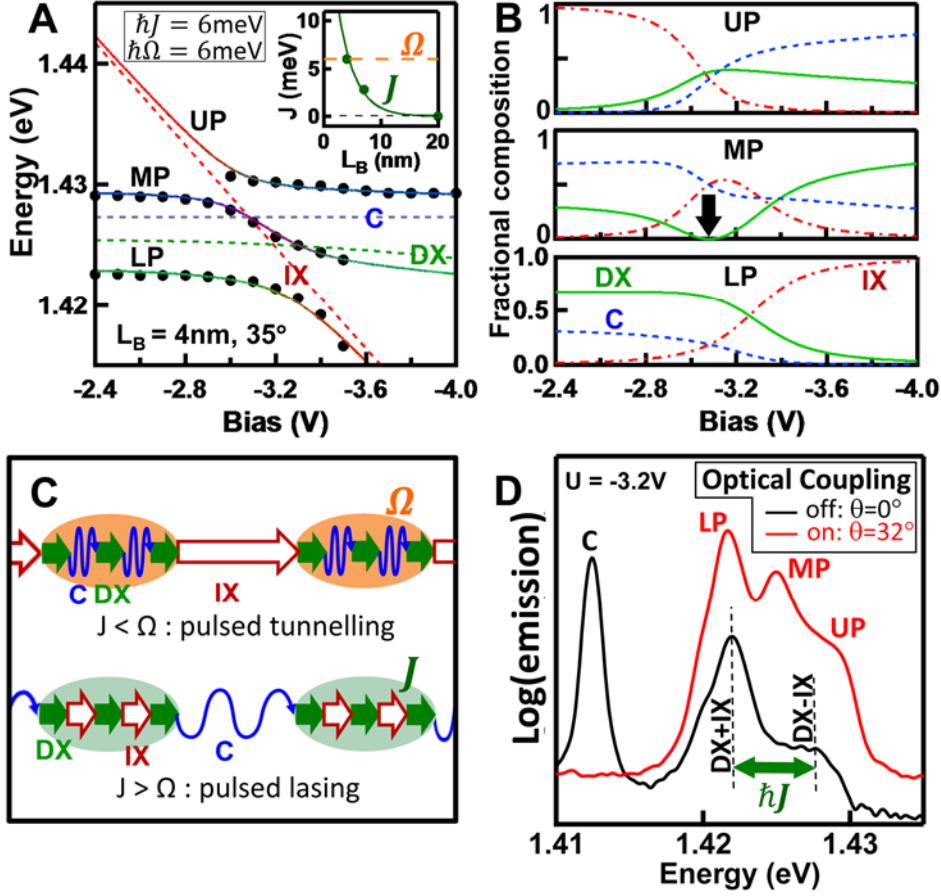
Fig. 3. (**A**) Bias-dependent polariton modes observed in photoluminescence for L_B = 4 nm with fits to the coupled oscillator model Eq. 1. Inset: extracted intrinsic tunneling rate J as a function of the barrier width (points) together with theory (line). (**B**) Bias dependence of the polariton composition; black arrow for MP marks position of the pure dipolariton of Eq. 2. (**C**) For $J < \Omega$, tunneling is suppressed while for $J > \Omega$ the Rabi frequency is reduced. (**D**) Optical control of the dipolariton regime by changing from red-detuned cavity (black) to resonance (red) through angle tuning.

$+\delta$) are

$$|MP\rangle = \alpha\{\Omega|IX\rangle - J|C\rangle\} \quad (2)$$

$$\begin{vmatrix} UP \\ LP \end{vmatrix} = \beta\{J|IX\rangle + \Omega|C\rangle + (\delta \pm S)|DX\rangle\} \quad (3)$$

Remarkably, while the central MP has no DX admixture at resonance (independent of the detuning δ) it is clearly visible in emission through the tunneling interaction with the cavity photon (and almost as strong as the other dipolaritons). The absence of DX in the MP arises from the destructive interference of transition amplitudes, as seen in Fig. 3B which shows the composition of each of the dipolariton modes versus bias, extracted from the coupled oscillator model of Fig. 3A. With increasing field the MP turns from an ordinary DX-polariton to a pure dipolariton at resonance (black arrow), consisting only of $|IX\rangle$ and $|C\rangle$ (Eq. 2), with the electron and hole located in different QWs and possessing a static dipole moment oriented perpendicularly to the QW plane (Fig. 1B).

In atomic physics this state is known as a dark polariton (*14*, *15*) and is employed for electromagnetically induced transparency (EIT) (*17*) in atomic media or waveguides (*18*), to drastically slow down light (*19*) and for light storage (*20*, *21*). The MP dipolariton differs from atomic dark polaritons in that the role of the second probe laser in the Λ-scheme is now taken by the bias-controlled electron tunneling transition. Applying EIT to a condensed dipolariton population could thus map photonic states onto electron tunneling states that can be read out in charge transport. This suggests new strategies for quantum readout and optical interconnects, for example as a variable pulse delay element in dipolariton signal processing. Furthermore, interactions between dipolaritons with vertically-aligned dipole moments are much stronger (by a factor 100) than for typical dipole-dipole scattering between in-plane excitons (*22*), and resemble an ensemble of Rydberg atoms in an electric field (*23*). The stronger repulsion of dipolaritons over conventional polaritons leads to increased stimulated scattering rates, and hence lower condensation thresholds (*22*). We suggest this is a fruitful approach to access room temperature polariton condensates.

The bare tunneling rate J controls the coupling between the two exciton modes and is set by the width and height of the barrier between the QWs. To test the tunnel control of dipolaritons, devices with barrier widths of 4nm, 7nm and 20nm were fabricated. Emission PL measurements (Fig. 3A and fig. S2) confirm the dependence of strong coupling dipolariton modes on this tunneling rate. Extracting the polariton Rabi splittings from each sample gives $\hbar\Omega$ = 6.0 meV while the tunnel splitting varies from $\hbar J = 0$ to 6meV (Fig. 3A, inset), proving that small tunnnelling barriers L_B are required to see dipolaritons. The tunnel splitting J exactly matches (Fig. 3A inset, line) that from parameter-free solutions of the Schrödinger equation for this asymmetric double QW with electric field (*13*), showing the expected exponential decrease in splitting with increased barrier width. The excellent fits confirm the simple explanatory power of this model for the observed modes.

Resonant dipolariton systems offer new ways to control tunneling. When Rabi flopping is faster than tunneling ($J < \Omega$), the dipolariton spends half of the time rapidly oscillating between a cavity photon and a

geometry. Diagonalisation of H yields the three dipolaritons modes $|LP\rangle$, $|MP\rangle$ and $|UP\rangle$, which provide an excellent account of the PL (Fig. 2, A and B, and Fig. 3A, solid lines, with uncoupled modes dashed).

At normal incidence (Fig. 2, A and C) the cavity mode is detuned 10meV below the excitons and hence effectively decoupled from the excitons. The weak exciton PL nevertheless directly resolves their tunnel splitting $\hbar J$ at the anti-crossing bias $U = -3.2$V (Fig. 3D, black curve). This situation changes at high angle (Fig. 2, B and D) where the cavity mode is resonant with both the direct and indirect exciton transition. For low bias voltage the IX is far detuned and the system behaves as a single-QW microcavity with direct excitons only, producing detuned Rabi splitting $\Omega' = \sqrt{\Omega^2 + \delta^2}$, where $\delta(U,\theta)$ is the detuning of DX below C at each bias and angle. Simultaneous resonance of DX, IX and the cavity mode is reached again at $U = -3.2$V and appears as three clearly distinct dipolariton branches spanned by an anti-crossing of width $S = \sqrt{\Omega'^2 + J^2}$. The eigenvectors at resonance (when $\omega C = \omega IX = \omega DX$

DX (Fig. 3C). Since for the time when the excitation is a cavity photon it is not available for tunneling, this results in a reduced effective tunneling rate $J_{\mathrm{eff}} = J/\sqrt{2}$. On the other hand in the fast tunneling limit $J > \Omega$, the electron is only in the left QW for half the time, which reduces the coupling to the cavity photon and hence the effective Rabi splitting. Thus, modifying the admixture of C and DX in MP allows optical control of the tunneling process: optical and electrical detunings determine the amount of time the electron spends shuttling between the left and right QWs or Rabi flopping on the DX transition. The anticrossings in the energy dispersion of LP-MP and MP-UP (figs. S4 and S5) quantify this effective tunneling rate J_{eff}, depending on J, Ω and detunings between the modes.

Such polariton mesas can be sensitively switched (fig. S3), toggling between the regimes of conventional polaritons and of strongly tunnel-coupled dipolaritons with a small change in bias voltage U (Fig. 1D) or of cavity angle θ (Fig. 3D). Furthermore, electrical manipulation of the coupling of the dipolariton static dipole moment to light is possible (fig. S5D).

In conclusion, the clear observation and control of dipolaritons in these electrical devices opens up interesting regimes for quantum optoelectronics, combining quantum tunneling with light-matter coupling. The full control of the modes in this system (with bias- and angle-tuning), together with the enhancement of dipolariton repulsion compared to conventional microcavity polaritons, implies they are strong candidates for high temperature condensates with tuneable interactions. The pure dipolariton EIT state, consisting only of cavity and indirect exciton components, offers a Λ transition scheme amenable to building coherence between light and matter states, directly applicable to novel transfer adiabatic schemes.

References and Notes

1. J. Kasprzak et al., Bose-Einstein condensation of exciton polaritons. *Nature* **443**, 409 (2006). doi:10.1038/nature05131 Medline
2. S. Christopoulos et al., Room-temperature polariton lasing in semiconductor microcavities. *Phys. Rev. Lett.* **98**, 126405 (2007). doi:10.1103/PhysRevLett.98.126405 Medline
3. R. Balili, V. Hartwell, D. Snoke, L. Pfeiffer, K. West, Bose-Einstein condensation of microcavity polaritons in a trap. *Science* **316**, 1007 (2007). doi:10.1126/science.1140990 Medline
4. K. G. Lagoudakis, B. Pietka, M. Wouters, R. André, B. Deveaud-Plédran, Coherent oscillations in an exciton-polariton Josephson junction. *Phys. Rev. Lett.* **105**, 120403 (2010). doi:10.1103/PhysRevLett.105.120403 Medline
5. A. Amo et al., Collective fluid dynamics of a polariton condensate in a semiconductor microcavity. *Nature* **457**, 291 (2009). doi:10.1038/nature07640 Medline
6. F. Capasso, Band-gap engineering: From physics and materials to new semiconductor devices. *Science* **235**, 172 (1987). doi:10.1126/science.235.4785.172 Medline
7. S. I. Tsintzos, N. T. Pelekanos, G. Konstantinidis, Z. Hatzopoulos, P. G. Savvidis, A GaAs polariton light-emitting diode operating near room temperature. *Nature* **453**, 372 (2008). doi:10.1038/nature06979 Medline
8. Z. Vörös, D. W. Snoke, L. Pfeiffer, K. West, Direct measurement of exciton-exciton interaction energy. *Phys. Rev. Lett.* **103**, 016403 (2009). doi:10.1103/PhysRevLett.103.016403 Medline
9. A. A. High, E. E. Novitskaya, L. V. Butov, M. Hanson, A. C. Gossard, Control of exciton fluxes in an excitonic integrated circuit. *Science* **321**, 229 (2008). doi:10.1126/science.1157845 Medline
10. G. Schinner et al., Electrostatically trapping indirect excitons in coupled $In_xGa_{1-x}As$ quantum wells. *Phys. Rev. B* **83**, 165308 (2011). doi:10.1103/PhysRevB.83.165308
11. M. Poggio et al., Spin transfer and coherence in coupled quantum wells. *Phys. Rev. B* **70**, 121305 (2004). doi:10.1103/PhysRevB.70.121305
12. G. Christmann et al., Control of polariton scattering in resonant-tunneling double-quantum-well semiconductor microcavities. *Phys. Rev. B* **82**, 113308 (2010). doi:10.1103/PhysRevB.82.113308
13. G. Christmann et al., Oriented polaritons in strongly-coupled asymmetric double quantum well microcavities. *Appl. Phys. Lett.* **98**, 081111 (2011). doi:10.1063/1.3559909
14. M. Fleischhauer, M. D. Lukin, Dark-state polaritons in electromagnetically induced transparency. *Phys. Rev. Lett.* **84**, 5094 (2000). doi:10.1103/PhysRevLett.84.5094 Medline
15. M. D. Lukin, S. F. Yelin, M. Fleischhauer, Entanglement of atomic ensembles by trapping correlated photon states. *Phys. Rev. Lett.* **84**, 4232 (2000). doi:10.1103/PhysRevLett.84.4232 Medline
16. The minimal splitting between LP and MP in Fig. 2A illustrates the absence of direct coupling between the IX and C, justifying $H_{13} = H_{31} = 0$ in Eq. 1.
17. M. Mücke et al., Electromagnetically induced transparency with single atoms in a cavity. *Nature* **465**, 755 (2010). doi:10.1038/nature09093 Medline
18. M. F. Yanik, W. Suh, Z. Wang, S. Fan, Stopping light in a waveguide with an all-optical analog of electromagnetically induced transparency. *Phys. Rev. resonance (red) through angle tuning.Lett.* **93**, 233903 (2004). doi:10.1103/PhysRevLett.93.233903 Medline
19. M. D. Lukin, A. Imamoğlu, Controlling photons using electromagnetically induced transparency. *Nature* **413**, 273 (2001). doi:10.1038/35095000 Medline
20. D. F. Phillips, A. Fleischhauer, A. Mair, R. L. Walsworth, M. D. Lukin, Storage of light in atomic vapor. *Phys. Rev. Lett.* **86**, 783 (2001). doi:10.1103/PhysRevLett.86.783 Medline
21. C. Liu, Z. Dutton, C. H. Behroozi, L. V. Hau, Observation of coherent optical information storage in an atomic medium using halted light pulses. *Nature* **409**, 490 (2001). doi:10.1038/35054017 Medline
22. A. Filinov, N. V. Prokof'ev, M. Bonitz, Berezinskii-Kosterlitz-Thouless transition in two-dimensional dipole systems. *Phys. Rev. Lett.* **105**, 070401 (2010). doi:10.1103/PhysRevLett.105.070401 Medline
23. D. Møller, L. B. Madsen, K. Mølmer, Quantum gates and multiparticle entanglement by Rydberg excitation blockade and adiabatic passage. *Phys. Rev. Lett.* **100**, 170504 (2008). doi:10.1103/PhysRevLett.100.170504 Medline

Supporting Online Material
www.sciencemag.org/cgi/content/full/science.1219010/DC1
Materials and Methods
Figs. S1 to S5
Reference (*24*)

11 January 2012; accepted 20 March 2012

Published online 5 April 2012; 10.1126/science.1219010
10.1126/science.1219010